



EVALUATION OF BACK TRAJECTORIES ASSOCIATED WITH OZONE TRANSPORT DURING THE 1993 NORTH ATLANTIC REGIONAL EXPERIMENT

JEROME D. FAST and CARL M. BERKOWITZ

Pacific Northwest National Laboratory, Richland, WA 99352, U.S.A.

(First received 6 June 1996 and in final form 9 August 1996)

Abstract—Back trajectories traditionally have been used to identify possible sources of pollutants measured at a receptor location; however, they neglect turbulent diffusion processes that affect pollutant transport. After evaluating the performance of a coupled mesoscale and Lagrangian particle dispersion model with observations taken during the 1993 Northern Atlantic Regional Experiment (NARE), a series of forward and back trajectories are analyzed to determine the errors associated with the back trajectory calculations. The forward trajectories are based on the mean and turbulent wind components and their initial positions correspond to several urban areas in eastern North America. The back trajectories employ only the mean wind components and their initial positions correspond to the final positions of the forward trajectories within a sampling volume near Yarmouth, Nova Scotia. Large differences between the forward and back trajectory positions occurred since the back trajectories did not include the irreversible turbulent diffusion processes. The back trajectories had no mechanism to identify surface source regions, with the consequence that the back trajectories would either pass over the “true” source region, or miss it altogether as a result of locating the particle at an incorrect horizontal position. A horizontal displacement error of ± 100 –400 km and a vertical displacement error of ± 0.2 –1 km occurred after 2 days of transport. These errors leveled off between 2 and 3 days, but grew larger again after 3 days of transport. The model results suggest that the use of back trajectories by themselves may be an inappropriate approach for estimating the source location of a plume emitted near the surface. Copyright © 1996 Elsevier Science Ltd

Key word index: Trajectory, long-range transport, boundary layer processes, turbulence, diffusion, meso-scale model, Lagrangian model.

1. INTRODUCTION

Back trajectories have long been a standard tool in air-quality studies for characterizing source–receptor relationships in air pollution field campaigns, examining meteorological mechanisms associated with pollutant observations, and establishing time scales for various chemical reactions. Forward and back trajectories are also very useful in describing the atmospheric dynamics of various weather systems. There are, therefore, many reasons to establish the confidence levels of trajectory calculations.

While the calculation of trajectories is straightforward, many uncertainties in the results arise from the input meteorological fields and the numerical methods. Several studies have been performed to examine the uncertainties due to the spatial and temporal resolution of the wind field. Draxler (1987) and Kahl and Samson (1986, 1988) used analyses based on standard and supplementary rawinsonde observations during the Cross Appalachian Tracer Experiment (CAPTEX) to demonstrate the differences in the trajectories due to spatial and temporal resolution of the observed wind field. Chock and Kuo (1990), in

their study of the Cross Appalachian Tracer Experiment (CAPTEX), and Draxler (1991), in his analysis of the Across North America Tracer Experiment (ANATEX), both found that numerical model output produced more accurate trajectories than low-resolution meteorological observations. Modeling approaches to evaluate the sensitivity of the trajectory to the spatial and temporal resolution of the meteorological fields has been examined by Doty and Perkey (1993), Kuo *et al.* (1985), Rolph and Draxler (1990), and Stohl *et al.* (1995). The role of vertical velocity in model calculations of trajectories for long-range transport was described by Martin *et al.* (1987). Haagensohn *et al.* (1990) demonstrated that improved trajectories could be obtained for ANATEX by combining numerical model output with observations using four-dimensional data assimilation. As described in Seibert (1993) and Stohl *et al.* (1995), errors associated with the spatial and temporal interpolation of the wind field can also lead to uncertainties in the trajectory calculations. Back trajectory errors calculated from large-scale numerical model output were evaluated by McQueen and Draxler (1994) using satellite images of the smoke plumes from the Kuwait oil fires.

These uncertainties are important to consider since many recent air quality studies have employed back trajectories to determine source regions of pollutants measured at receptor locations. For instance, Stohl and Kromp-Kolb (1994) utilized low-level back trajectories to determine source regions for ozone observed in Vienna, Austria. Back trajectories originating in Alpine valleys were calculated by Graber *et al.* (1995) using a high-resolution modeling system to determine the influence of the Alps on the production of photo-oxidants. Mukai *et al.* (1994) employed a back trajectory analysis and found that lead isotope ratios in airborne particulate matter were a good indicator of the long-range transport of pollutants in eastern Asia. Measurements in Bermuda and 10-day back trajectories were made by Dickerson *et al.* (1995) to illustrate the long-range transport of pollutants over the Atlantic Ocean. Van Dingenen (1995) used black carbon as a tracer and a back trajectory analysis to find that anthropogenic sulfate advected from continental regions contributed to sulfate over the Atlantic Ocean. Back trajectories were used by Jacob *et al.* (1995) and Moy *et al.* (1994) to determine possible source regions of carbon monoxide, ozone, and total reactive nitrogen oxides observed in Shenandoah National Park in Virginia.

Trajectory calculations have also been employed by several recent studies using meteorological and air pollution measurements taken during the 1992 and 1993 North Atlantic Regional Experiment (NARE) field campaigns. In these studies, back trajectories were used to demonstrate the effect of vertical wind shears in determining potential source regions (Angevine *et al.*, 1996), correlate high ozone events with major urban and industrial sources located in the central and eastern U.S. (Kleinman *et al.*, 1996a), and illustrate the role of cyclonic systems in transporting pollutants within the warm sector ahead of cold fronts (Berkowitz *et al.*, 1996). Forward trajectories produced by a coupled mesoscale model and Lagrangian particle dispersion model showed that mixing of particles released from multiple urban areas results in a plume over Nova Scotia that is characterized by a distribution of ages and sources which vary with altitude (Fast and Berkowitz, 1996). This modeling system also demonstrated that the layering of pollutants is well established prior to the air masses leaving land by convective boundary-layer processes, vertical wind shears, and synoptic-scale vertical motions.

Most of the studies previously mentioned have assumed that pollutant transport as described by the trajectories is the result of pure advection with no turbulent diffusion processes. While diffusion processes can be simulated by various types of forward dispersion models, the effects due to diffusion cannot be incorporated into back trajectories because turbulence is an irreversible process. In contrast to previous trajectory sensitivity studies, a modeling approach is used in this paper to evaluate the effect of neglecting

turbulence processes on back trajectory calculations. The spatial differences between forward and back trajectories, as a function of time and distance from the receptor location, are computed using data collected during the 1993 NARE field campaign. More general quantitative statistics derived from thousands of forward/backward trajectory pairs are then presented to demonstrate the importance of turbulent diffusion processes.

2. CASE STUDY

The basis of our investigation into the effect of turbulent diffusion processes on the calculation of back trajectories is a series of measurements collected by the National Research Council of Canada's Twin Otter aircraft as part of the 1993 North Atlantic Regional Experiment (NARE). As described by Kleinman *et al.* (1996a,b), 45 sampling missions within 50 km of Yarmouth, Nova Scotia were made by the Twin Otter aircraft over a 34-day period between 6 August and 8 September 1993. Sampling was done from near the surface to either 3 or 5 km, with relatively complete daily coverage below 3 km. Elevated layers of ozone and other chemical species were observed with peak ozone mixing ratios frequently occurring between 0.8 and 1.5 km above the ocean. Only in a few instances did the peak ozone mixing ratio occur near the surface. The highest ozone mixing ratios were strongly correlated with southwesterly winds during this period; however, southwesterly winds were not always associated with high ozone mixing ratios (Kleinman *et al.*, 1996a). The summer climatology of the region suggests that southwesterly winds associated with high-pressure systems may transport ozone from the U.S. east coast urban corridor towards the east, eventually affecting the air quality and influencing the mass budget of ozone and related species over the western North Atlantic (Berkowitz *et al.*, 1996). Other field experiments have shown that high concentrations of ozone frequently occur in the vicinity of Nova Scotia (Parrish *et al.*, 1993; Berkowitz *et al.*, 1995). Studies of this phenomenon have focused on the chemistry of pollutant plumes (Daum *et al.*, 1996; Kleinman *et al.*, 1996a,b) and the associated synoptic-scale meteorology (Anderson *et al.*, 1993; Berkowitz *et al.*, 1996).

The 850 mb geopotential height fields and the surface analyses between 25 August and 2 September 1993 are shown in Fig. 1. During this period, a series of low-pressure centers moved through the northcentral U.S., over eastern Canada, and out over the North Atlantic while a high pressure system dominated the southern U.S. and western Atlantic. The trough on 25 August (Fig. 1a) and the cold fronts on 29 August (Fig. 1e) and 1 September (Fig. 1h) were all preceded by strong westerly to southwesterly winds. Since there are no significant sources of pollutants in the vicinity of Yarmouth, previous investigators have

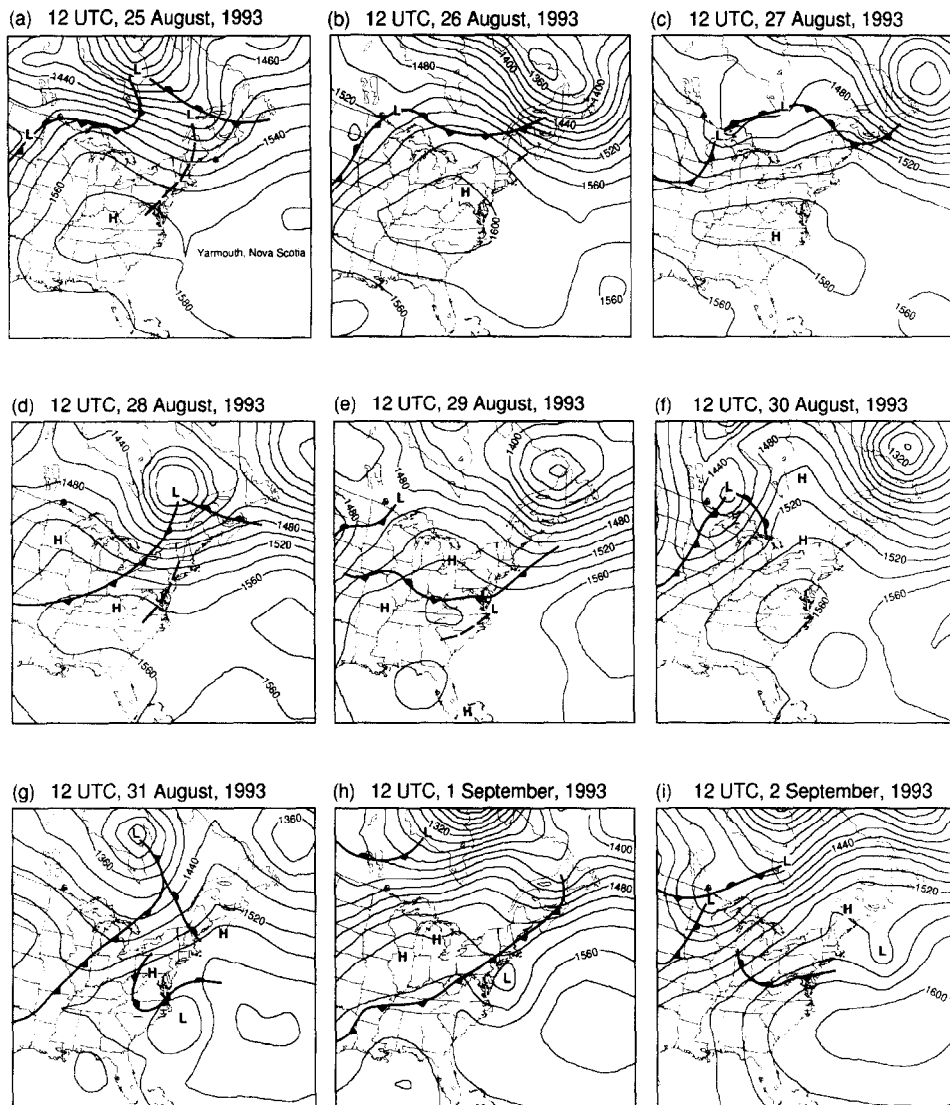


Fig. 1. 850 mb geopotential heights (contour interval of 20 m) and positions of surface fronts, high and low pressure systems at the 12 UTC periods between 25 August and 2 September during the 1993 NARE field campaign.

concluded that high ozone mixing ratios observed during this period were due to emissions of ozone precursors over the U.S. that were advected over the western North Atlantic by the large-scale winds associated with the synoptic systems depicted in Fig. 1. The polluted air over Nova Scotia was subsequently replaced by relatively clean air masses originating from Canada after the passage of low-pressure systems. A detailed description of the boundary-layer processes and trajectories during this period are given in Fast and Berkowitz (1996). The ozone data from the NARE field campaign will be presented in this paper only to establish that the modeling system used in the evaluation of forward trajectories yields results consistent with the observations.

3. MODEL DESCRIPTION

3.1. Mesoscale model

The Regional Atmospheric Modeling System (RAMS) (Pielke *et al.*, 1992) is used to predict the synoptic and mesoscale flow features during a portion of the 1993 NARE field campaign as described by Fast and Berkowitz (1996). The turbulence parameterization consists of a simplified second-order closure method that employs a level-2 diagnostic scheme or a level-2.5 scheme with a prognostic turbulence kinetic energy equation as proposed by Mellor and Yamada (1982) and modified for the case of growing turbulence according to Helfand and Labraga (1988).

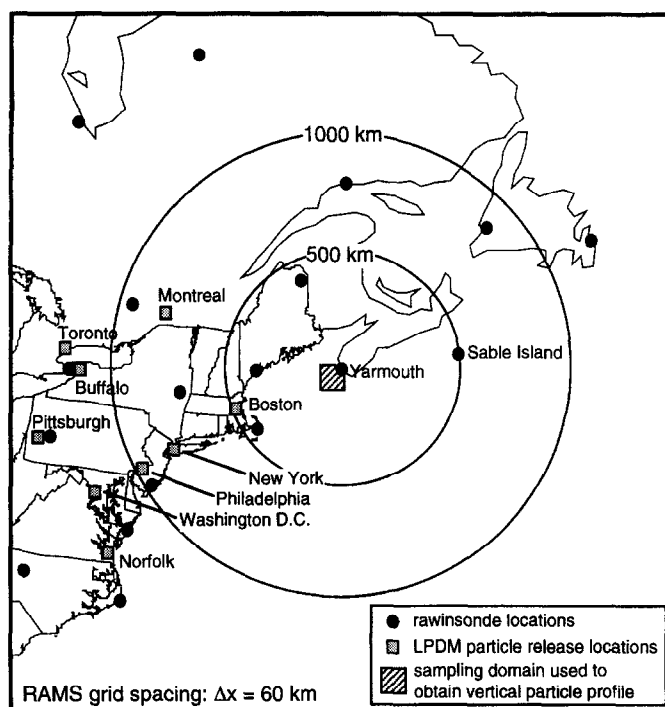


Fig. 2. Modeling domain, rawinsonde locations, and urban area release sites for the particle dispersion model. Concentric rings indicate distances from Yarmouth, Nova Scotia.

The model domain shown in Fig. 2 is designed to resolve the circulations responsible for pollutant transport during the NARE field study period. A horizontal grid spacing of 60 km is used (44×46 grid points). This grid spacing is sufficient to resolve mid-latitude synoptic systems. A stretched terrain-following vertical coordinate is employed with a grid spacing of 50 m adjacent to the surface. Between 50 and 1550 m above ground level (AGL), the grid spacing is 100 m. Above 1550 m, the grid spacing gradually increases to 1000 m near the model top at an elevation of 17.9 km AGL. Due to the staggered coordinate system, the lowest model vertical coordinate is located about 26 m AGL. With this vertical resolution, 17 grid points are positioned within 1550 m of the ground to resolve boundary-layer processes responsible for pollutant transport from surface releases.

The initial conditions for RAMS are an analysis based on the global fields from the National Center for Environmental Prediction (NCEP) Medium Range Forecast (MRF) model and the rawinsonde observations from the National Weather Service (NWS). Additional analyses using MRF model output and observations are made at each 00 and 12 UTC period. These analyses and the MRF 6 h forecasts for the 06 and 18 UTC periods are used to provide the time-dependent lateral boundary conditions for RAMS during the simulation period. The forcing at the lateral boundaries is applied on the outermost five

grid points and the magnitude of the forcing varies linearly in time between 6 h intervals. Sea-surface temperatures are obtained by interpolating a two-week composite analysis with a 1° horizontal resolution to the ocean grid points.

A critical component in the description of long-range pollutant transport is the specification of the wind field. Four-dimensional data assimilation (FDDA) techniques (Harms *et al.*, 1992) provide a method for incorporating meteorological observations into the model results over an extended period of time. FDDA is used in this study to reduce the uncertainties associated with pollutant transport by limiting the error growth in the wind, temperature, and moisture fields. A Newtonian (nudging) FDDA technique is incorporated in RAMS (Fast, 1995; Stauffer and Seaman, 1994) to bring the prognostic variables (u - and v -component of the wind, potential temperature, and specific humidity) into closer agreement with 19 rawinsonde observation profiles (Fig. 2) throughout the simulation period. Therefore, the mesoscale model results are a blend of the observations and the forecasts close to the 00 and 12 UTC periods and the atmospheric fields are based mostly on the forecasts between these periods. Only 2 rawinsondes are located on islands so that the atmospheric fields are based primarily on model forecasts over the ocean areas of the domain in Fig. 2. Additional details of the FDDA procedure can be found in Fast and Berkowitz (1996) and Fast (1995).

3.2. Lagrangian particle dispersion model

A Lagrangian particle dispersion Model (LPDM) described by Fast *et al.* (1995) is used to simulate pollutant dispersion during the 1993 NARE field campaign. Atmospheric dispersion is simulated by tracking a large number of particle positions based on the mean velocity component produced by RAMS and a sub-grid scale turbulent velocity component. The position of each particle is given as

$$x(t + \Delta t) = x(t) + (\bar{u}(t) + \tilde{u}(t))\Delta t \quad (1)$$

$$y(t + \Delta t) = y(t) + (\bar{v}(t) + \tilde{v}(t))\Delta t \quad (2)$$

$$z(t + \Delta t) = z(t) + (\bar{w}(t) + \tilde{w}(t))\Delta t \quad (3)$$

where x , y , and z are the spatial coordinates and Δt is the time step. LPDM has been modified to include the Thomson formulation of the equation for the turbulent vertical velocity component as described in Hurlley and Physick (1991). The subgrid scale turbulent velocity components, \tilde{u} , \tilde{v} , and \tilde{w} are computed by solving the Langevin equation by a Markov-chain formulation (Legg and Raupach, 1982) and depend upon the values at the previous time step according to

$$\begin{aligned} \tilde{u}(t) = & R_u \tilde{u}(t - \Delta t) + \sqrt{(1 - R_u)} \sigma_u \eta_u \\ & + \tau_u (1 - R_u) \frac{\partial \overline{u'w'}}{\partial z} \end{aligned} \quad (4)$$

$$\begin{aligned} \tilde{v}(t) = & R_v \tilde{v}(t - \Delta t) + \sqrt{(1 - R_v)} \sigma_v \eta_v \\ & + \tau_v (1 - R_v) \frac{\partial \overline{v'w'}}{\partial z} \end{aligned} \quad (5)$$

$$\begin{aligned} \tilde{w}(t) = & R_w \tilde{w}(t - \Delta t) + \sqrt{(1 - R_w)} \sigma_w \eta_w \\ & + \tau_w (1 - R_w) \frac{1}{2} \frac{\partial \sigma_w^2}{\partial z} + \tau_w (1 - R_w) \\ & \times \frac{\tilde{w}(t - \Delta t)^2}{2\sigma_w^2} \frac{\partial \sigma_w^2}{\partial z} \end{aligned} \quad (6)$$

where R_i is the autocorrelation coefficient (the subscript i is either u , v , or w), t_i the Lagrangian time scale, and σ_i the standard deviation of the turbulent velocities. The values of η_i are randomly chosen out of a normalized Gaussian distribution. The variances and covariances (σ_i , $\overline{u'w'}$, and $\overline{v'w'}$) are obtained from the mesoscale model and are consistent with the second-order closure applied in RAMS.

In this study, the mean velocity field employed by LPDM is based on output produced by the mesoscale model at 2 h intervals. LPDM linearly interpolates the mean velocity field in time during individual 2 h periods using a time step, Δt , of 15 s. Particles are non-buoyant and a perfect reflection of particles occurs at the ground; deposition is not included in this study. Each particle is tagged by its location, release location, and release time so that the history of a particle plume and forward trajectories can be derived at any time. Back trajectories are calculated by running

the model backwards and setting \tilde{u} , \tilde{v} , \tilde{w} in equations (1)–(3) to zero.

4. EXPERIMENTAL METHOD

4.1. Forward dispersion analysis

The mesoscale model and the Lagrangian particle dispersion model are used to simulate the structure of the ozone mixing ratio profiles observed over Yarmouth for a 15 day period between 12 UTC 18 August and 12 UTC 2 September 1993. Three high-ozone mixing ratio events, referred to as "A", "B", and "C", occurred during this period that were correlated with other chemical species associated with urban emissions (Kleinman *et al.*, 1996a). Each event is separated by periods during which relatively small ozone mixing ratios were observed below 3 km.

The dispersion of pollutants is simulated in the Lagrangian particle dispersion model by tracking the path of thousands of particles released from several urban areas in North America. Nine release locations were selected (Fig. 2), including five major metropolitan areas located along the east coast urban corridor and four major metropolitan areas west of the Appalachian mountains. Particles are emitted at the surface at a constant rate throughout the 15 day period from the surface within an area of 900 km² at each location. The same release rate is used at each of the nine locations. Approximately, 385,000 particles are released over the 15 day period, although the maximum number of particles on the domain at any one time was about 107,000. The long simulation period also enables the individual particles to be tracked for a substantial period of time.

Model performance is evaluated by comparing the shape of the vertical profiles of simulated particle number density with the corresponding profiles of ozone mixing ratios measured by the Twin Otter aircraft. Particle profiles are obtained by counting particles within a fixed column of 100 cells located just southwest of Yarmouth (Fig. 2). The volume of each cell is 720 km³ (120 km × 120 km × 50 m) and the column of cells extends up to 5 km AGL. An instantaneous particle profile is obtained for this column every hour; no time averaging is performed. A height–time cross section showing the simulated particle concentrations over Yarmouth is presented in Fig. 3b. Relatively high particle concentrations, similar to events A, B, and C, are evident shortly before the passage of the low-pressure systems shown in Fig. 1. After the passage of cold fronts on 21 and 29 August, the particle plume is advected towards the south over the Atlantic, producing near-zero concentrations at Yarmouth that are similar to the low ozone mixing ratios observed by the Twin Otter at these times. The model results and the observations are in good agreement with the Twin Otter flights on and after 21 August.

Further evidence that the modeling system reproduces the regional-scale meteorology and transport during the period is shown in Fig. 4 which compares the particle profile within the sampling domain for three time periods with the observed aircraft profiles of ozone mixing ratio and aerosol concentration. The observed peak ozone mixing ratios and aerosol concentrations for events "A" and "C" are located between 0.5 and 1.5 km AGL, while they occur closer to the surface during event B. The good agreement in the shapes of the observed ozone and simulated particle profiles and the elevation at which the maxima occur suggests that meteorological processes are largely responsible for the layering of chemicals over Yarmouth and that following the paths of passive particles is very useful in illustrating these processes. Still, the observed ozone profiles and the simulated particle profiles can only be compared qualitatively since the Lagrangian model does not include chemical reactions that take place during the transport period and there is no background particle concentration comparable to ambient ozone

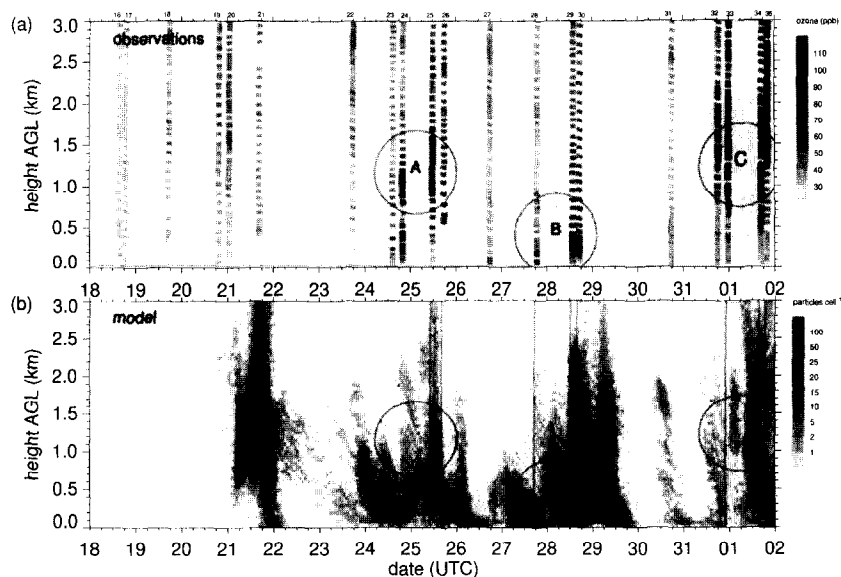


Fig. 3. (a) Observed profiles of ozone mixing ratios (shaded) from the Twin Otter aircraft along with the flight numbers and (b) simulated profiles of particle concentration (shaded) within the sampling domain over Yarmouth, Nova Scotia where the vertical lines indicate the times in which back trajectories are calculated. Circles A, B, and C denote periods and elevations in which high ozone mixing ratios were observed.

from non-anthropogenic sources. The lack of an ambient background particle concentration contributes to the small particle concentrations that are usually predicted above 2 km AGL. Fast and Berkowitz (1996) found that the peak concentrations within 3 km AGL of the ground resulted from inhomogeneous convective boundary layer processes over land and synoptic scale lifting in advance of the cold fronts and troughs depicted in Fig. 1. The near-surface winds generally had a more southerly component than the winds aloft during events A and C so that relatively clean air masses were present near the surface over Yarmouth. We will treat the forward trajectories of the particles as realistic representations of the circulation and transport features for this time period and compare them with a series of back trajectories.

4.2. Forward and back trajectory calculations

Forward trajectories are computed for each particle that enters the sampling domain at eight times between 25 August and 2 September corresponding to the aircraft flight periods, which resulted in a total of 7652 trajectories (a subset of the 385,000 total particle trajectories during the simulation period). Particle positions are updated every 15 s, but the positions of the particles are stored at 1 h intervals. The trajectories are classified into groups corresponding to the aircraft measurement periods, denoted by the vertical lines in Fig. 3b and listed in Table 1. Even though the particles are distributed throughout the vertical column up to 3 km AGL, most of the final trajectory heights occur close to the peak particle concentration levels (Figs 3b and 4).

Trajectories are not calculated at other times because no observational data are available to verify the structure of the predicted particle profile. Trajectories are not calculated for Twin Otter flights 27, 31, and 32 (Fig. 3a) since the number of particles entering the sampling domain is relatively small and the observations indicated relatively clean air masses at these times. As indicated by equations (1)–(6), both the mean velocities and turbulent diffusion processes affect the paths of the forward trajectories.

Back trajectories are then calculated for each forward trajectory. The initial position of each back trajectory is the final position (latitude, longitude, elevation, time) of a forward trajectory within the sampling domain. Back trajectory positions are determined by running LPDM in reverse using only the mean wind velocities in equations (1)–(3). Positions are updated and stored at hourly intervals. Calculations continue until the back trajectory falls outside of the domain or after 5 days have elapsed. The duration of almost all of the forward trajectories is less than 5 days.

Initial tests of LPDM using only the mean wind velocities for both the forward and back trajectories demonstrated that the numerical errors associated with trajectory calculations were very small so that the forward and back trajectories were nearly identical (not shown).

4.3. Error statistics

Two statistics are used in comparing the forward and back trajectories for the eight time periods. These are the absolute horizontal displacement difference (AHDD) and the absolute vertical displacement difference (AVDD) and are defined as

$$\text{AHDD} = \frac{1}{n_f(t)} \sum_{n=1}^{n_f(t)} [(x_f^n(t) - x_b^n(t))^2 + (y_f^n(t) - y_b^n(t))^2]^{0.5} \quad (7)$$

$$\text{AVDD}(t) = \frac{1}{n_f(t)} \sum_{n=1}^{n_f(t)} [(z_f^n(t) - z_b^n(t))^2]^{0.5} \quad (8)$$

where n_i is the total number of trajectories, n the trajectory number, and f and b denote forward or backward trajectories, respectively. Many investigators have employed statistics similar to equations (7) and (8) in evaluating the accuracy of trajectories (Doty and Perkey, 1993; Draxler, 1991; Kahl and Samson, 1988; Kuo *et al.*, 1985; Rolph and Draxler, 1990; Stohl *et al.*, 1995). These statistics are often referred to as the absolute horizontal (vertical) displacement error; how-

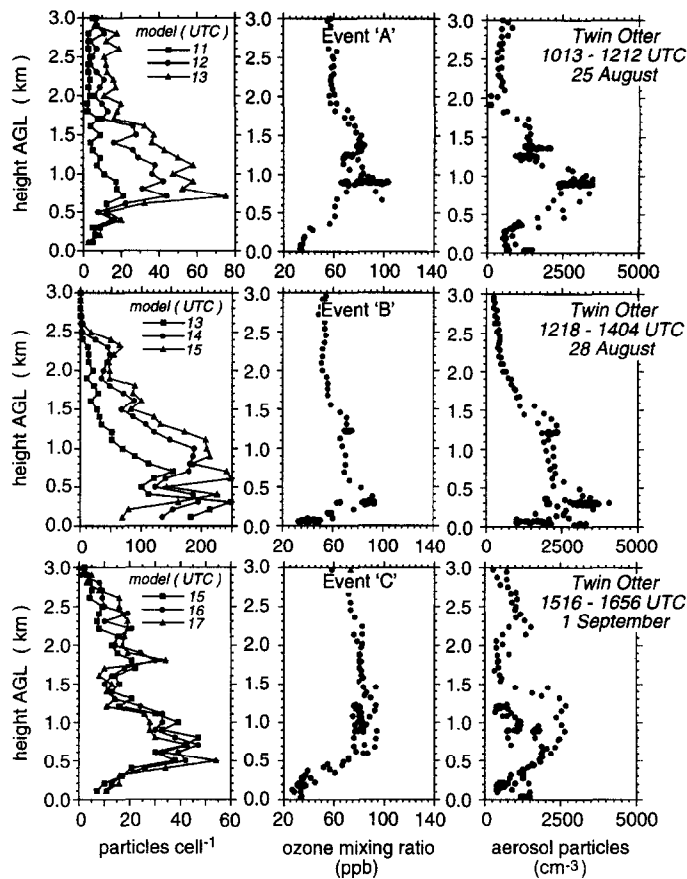


Fig. 4. Comparison of observed ozone and aerosol profiles from the Twin Otter aircraft with the simulated particle profile at three select time periods.

Table 1. Attributes of the trajectory groups corresponding to the Twin Otter flight times shown in Fig. 3

| Trajectory group | End time of forward trajectories and start time of back trajectories | Number of trajectories | Twin Otter aircraft flight number |
|------------------|----------------------------------------------------------------------|------------------------|-----------------------------------|
| A1 | 12 UTC, 25 August | 565 | 25 |
| A2 | 18 UTC, 25 August | 406 | 26 |
| B1 | 19 UTC, 27 August | 474 | 28 |
| B2 | 14 UTC, 28 August | 2647 | 29 |
| B3 | 16 UTC, 28 August | 2408 | 30 |
| C1 | 02 UTC, 1 September | 122 | 33 |
| C2 | 16 UTC, 1 September | 594 | 34 |
| C3 | 20 UTC, 1 September | 436 | 35 |

ever, tracer data need to be tracked from the source to the receptor to quantify the true errors associated with computed trajectories. Use of the word "error" in this study refers to the difference between the forward and back trajectories due to the omission of turbulence in the back trajectory calculation.

The length of time for a particle to reach the sampling domain from a source area via a forward trajectory need not be the same as the time required for a particle to leave the model domain via a back trajectory that begins at Yarmouth. When the transport period for the forward trajectory is less than the back trajectory transport period, the AHDD and AVDD assume that the forward trajectory position is

at the release location while the back trajectory continues towards the domain boundary. The evaluation of the displacement differences is terminated when the back trajectory leaves the model domain, which usually occurs in less than 5 days at middle and upper levels where the wind speeds are higher than at the surface. As a consequence, the number of trajectory pairs, n_t , decreases with time as the back trajectories leave the domain. While this places less confidence in the statistics with increasing time, there are still 66 and 34% of the total number of trajectories remaining after 4 and 5 days of transport, respectively. However, there are no trajectories left for trajectory groups B1 and C1 after 4 and 5 days of transport.

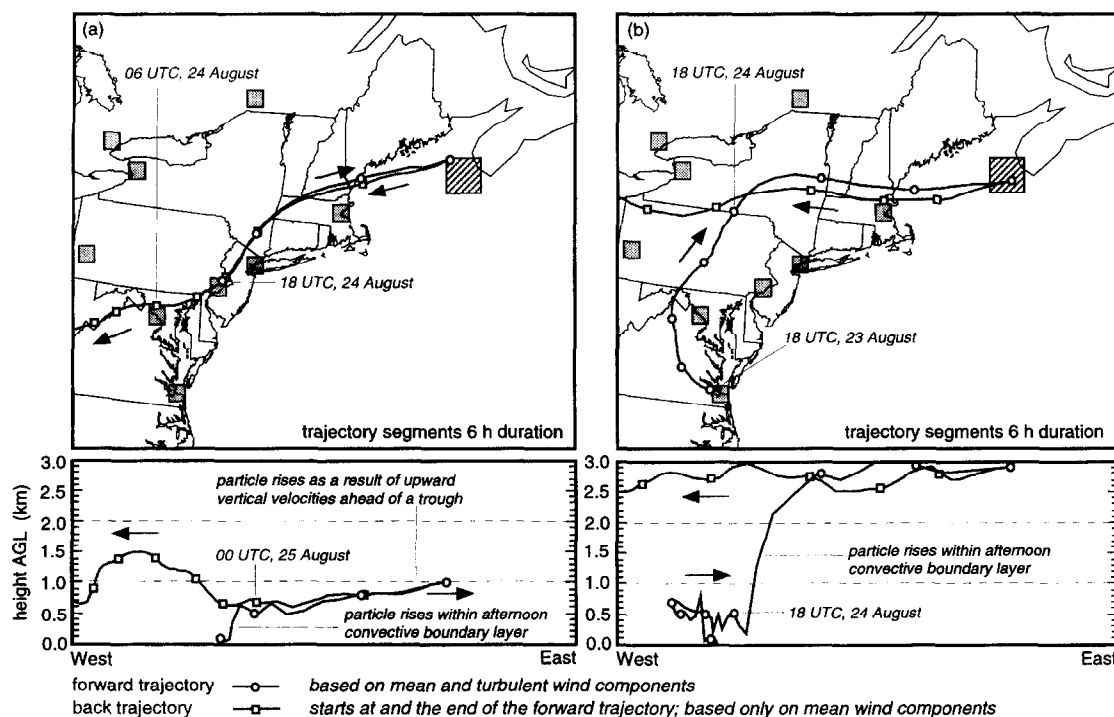


Fig. 5. Select forward trajectories terminating within the sampling domain at 12 UTC, 25 August during event A and the corresponding back trajectory. Symbols on the trajectories are plotted at 6 h intervals.

Since the wind speed varies in space and time, equations (7) and (8) do not provide information corresponding to distance from the sampling domain. AHDD and AVDD are also calculated as a function of distance from Yarmouth by obtaining the positions of each trajectory at constant 2 km intervals from Yarmouth.

5. RESULTS

5.1. Selected trajectories

Two representative forward trajectories during event A are shown in Fig. 5. For both of these trajectories convective boundary layer processes are responsible for mixing the particle upwards before it is advected by stronger westerly winds aloft into the sampling domain. In Fig. 5a, the back trajectory is nearly identical to the forward trajectory back to the release location in Philadelphia. This occurs because soon after the release the particle is quickly advected above the boundary layer where it remains for most of the transport period so that turbulence processes are small. The back trajectory, however, has no mechanism to transport the particle back down to the surface near the release location in Philadelphia since it was turbulence diffusion processes that initially mixed it upwards. Instead, the back trajectory continues until it intersects the domain boundary. In this case, a back trajectory calculation would correctly estimate the source region to be somewhere along the back trajectory, but the distance from the receptor could

not be determined unless there was a unique chemical signature to the measurements.

Particles that are released from Norfolk (Fig. 5b) are advected over New York by near-surface southerly winds associated with a high-pressure center located over southern New England on 23 August. As the particle in the forward trajectory is mixed upwards within the convective boundary layer, it is affected by vertical wind shears in which the winds aloft become more westerly with height. The back trajectory in this case indicates the source would be from the west, although the forward dispersion calculation illustrates that emissions from the southern locations can contribute to the pollutants at that level over Yarmouth. Relatively large horizontal and vertical errors in the back trajectory are produced 24 h prior to the sampling time.

Representative forward and back trajectories during event B are shown in Fig. 6. In these two cases, the back trajectories indicate sources to the west of Yarmouth; however, the forward dispersion calculation again demonstrates that it is possible to have contributions from sources located further to the south along the coast. The particle rises a few hundred meters just before arriving at Yarmouth due to synoptic-scale vertical motion associated with the approach of the trough and cold front on 28 August (Fig. 1d). This feature is also included in the back trajectory, since the back trajectory includes the mean vertical wind component. Nevertheless, relatively large hori-

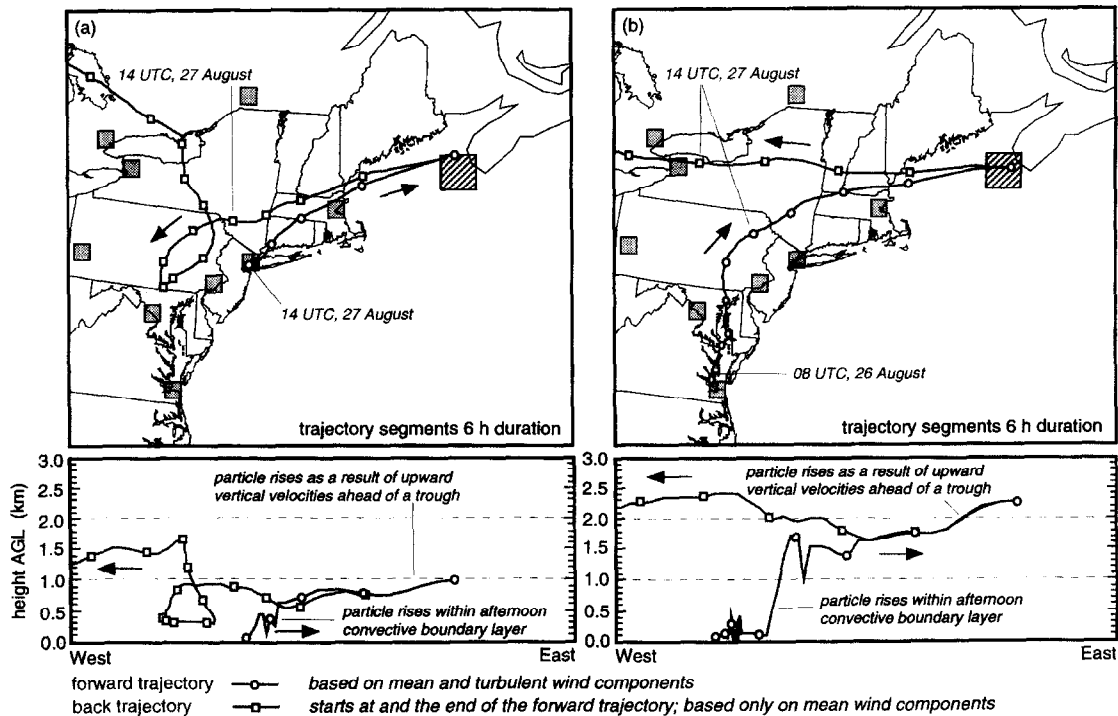


Fig. 6. Same as Fig. 5, except at 14 UTC, 29 August during event B.

zonal errors occur a few hundred kilometers from Yarmouth even above 1 km AGL (Fig. 6b). Some of the errors aloft above the boundary layer are due to the random term in equations (4)–(6) for stable boundary layers. Small errors can grow quite large over a relatively long period of time.

As shown by two representative trajectory pairs during event C in Fig. 7, a back trajectory calculation could lead to erroneous conclusions regarding the circulations that may be possible for the high levels of pollutants over Yarmouth. The back trajectory in Fig. 7a passes over the proper source (Boston), but the upper-level southwesterly wind causes the trajectory to continue into west Virginia. The particle released from Boston actually follows a circuitous path to Yarmouth in the forward dispersion process. This particle is transported within the clockwise circulation associated with the passage of a high-pressure system. During event C, the recirculation of pollutants over the northeastern coast of the U.S. was not uncommon. In Fig. 7b, the back trajectory indicates possible source regions in the urban areas of southern Canada; however, strong southerly winds ahead of the cold front on 31 August (Fig. 1g) advected a large fraction of particles near the surface into southern Canada before they were advected into the sampling domain in the forward dispersion process.

Figures 5–7 demonstrate that in the presence of large vertical wind shears, small vertical back trajectory position errors can gradually produce relatively large horizontal back trajectory position errors. The

trajectory pairs considered for events A, B and C are specific examples of the types of errors introduced into back trajectory calculations resulting from the omission of turbulent diffusion. In the following section, the effect of the turbulence diffusion processes on the overall statistics will be considered.

5.2. Trajectory errors

The horizontal and vertical displacement errors for all 7652 back trajectories are shown in Fig. 8. The AHDD and AVDD gradually grows with time so that after 48 h of transport the average horizontal and vertical errors are as large as 350 and 0.75 km, respectively. The average horizontal error increases to 500 km and the average vertical error increases to 1 km at 96 h of transport. When AHDD and AVDD are calculated as a function of distance, the errors also grow gradually with distance but the rate of growth of the horizontal and vertical errors decreases at approximately 1200 km from Yarmouth. This occurs because the paths of many of the forward and back trajectories approach each other and sometimes intersect before diverging again. Since all of the sources, except Boston, are located at a distance of 750–1250 km from Yarmouth, the omission of turbulent diffusion processes could lead to a horizontal back trajectory error over the source regions as large as 350 km (Fig. 8). The vertical errors as a function of distance (Fig. 8b) are rather small within 500 km of Yarmouth when most of the back trajectories are located over the ocean to the south and west of Nova Scotia. This is

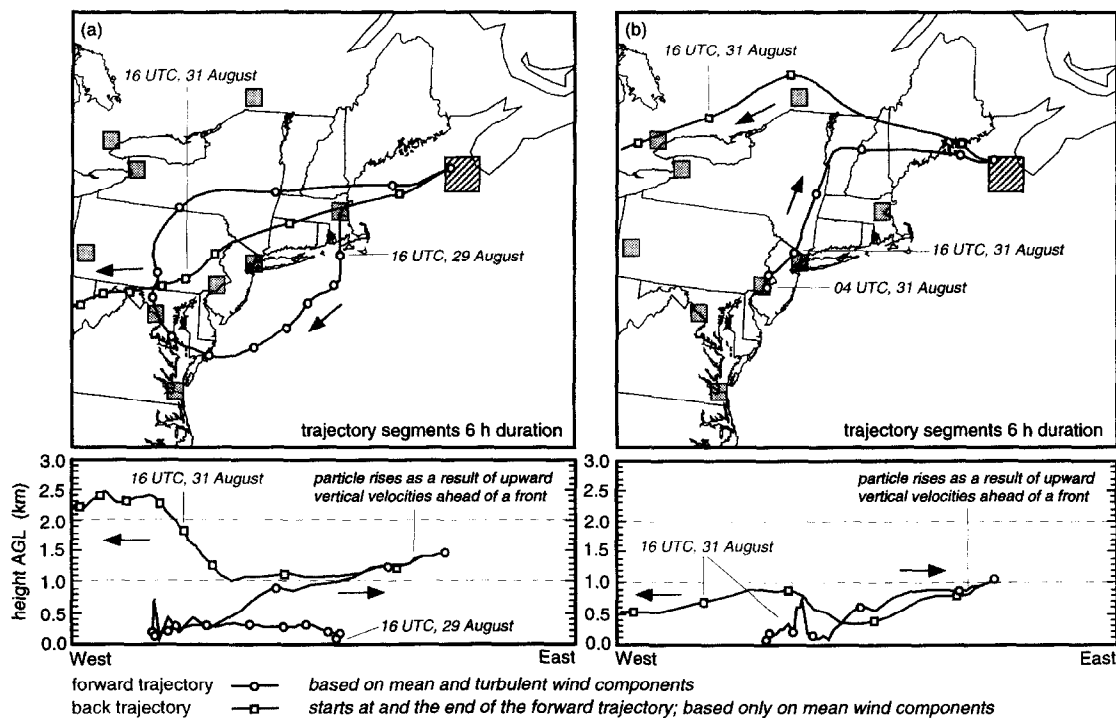


Fig. 7. Same as Fig. 5, except at 16 UTC, 1 September during event C.

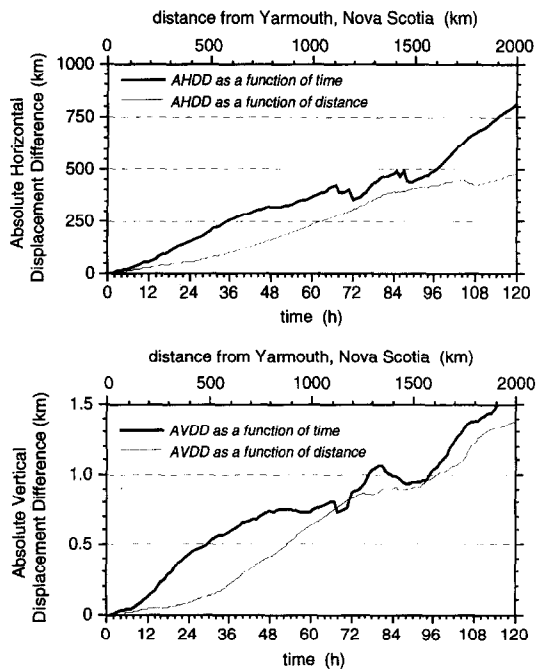


Fig. 8. Absolute horizontal displacement difference (AHDD) and absolute vertical displacement difference (AVDD) as a function of time and distance from Yarmouth, Nova Scotia.

consistent with the physically plausible expectation that the turbulent diffusion processes are small over the ocean areas within and above the marine bound-

ary layer. As soon as the back trajectories reach land, the AVDD increases dramatically.

While considerable variation in the differences between the forward and back trajectories can occur between each trajectory group, no clear systematic variation in the AHDD or AVDD was found for events A, B, or C making it difficult to assess the exact conditions under which back trajectories would *a priori* be expected to have relatively small errors. Relatively small horizontal errors are associated with trajectory groups B2 and B3 within 1500 km of Yarmouth that appear to be the result of the strong winds during event B. The relatively rapid transport during event B did not permit turbulence diffusion processes to affect the forward dispersion of particles as much as events A and C. A large fraction of the particles for trajectory groups A1, A2, C2, and C3 had long, complex routes due to high-pressure centers and light winds that dominated the eastern U.S. (Fig. 1) so that turbulent diffusion processes could affect the trajectories over a relatively long period of time. The depth of the convective boundary layer predicted by the model just prior to events A and C was also greater, in general, than for event B. Turbulent kinetic energy, and therefore the values of \bar{u} , \bar{v} , \bar{w} , in equations (4)–(6) will be larger when particles are located within a strong convective boundary layer.

The AHDD and AVDD are also calculated for all of the back trajectories as a function of the initial height at the receptor location. The statistics are grouped according to three layers using initial heights from 0 to 0.5, 0.5 to 1.5, and 1.5 to 3.0 km AGL and

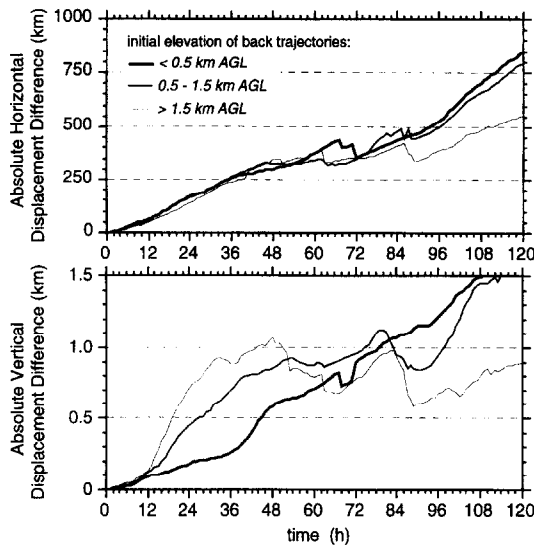


Fig. 9. AHDD and AVDD as a function of time and initial elevation of the back trajectories.

the results are given in Fig. 9. Although the horizontal errors for each layer are not significantly different for 60 h or less of transport, the upper-level back trajectories have slightly smaller errors after 84 h. The large

vertical errors for the upper-level back trajectories after only 12 h of transport arise because there is no mechanism to track the particle back down to its source at the surface as shown by Figs 5–7. The vertical positions of the particles are affected only by the mean vertical motions in the back trajectory calculations, and not by turbulence. The synoptic-scale vertical velocities are usually small so that the back trajectories do not vary much with height over a long period of time (Fig 5b, 6b, and 7b); therefore, vertical errors for the upper-level back trajectories can be quite large because the sources are located at the surface. During periods of strong downward mean vertical motions (Figs 5a, 6a, and 7a), large vertical errors are produced since the back trajectory is displaced further from the surface.

Figure 10 shows the corresponding AHDD and AVDD distribution for trajectory groups A1, B2, and C2. These distributions are representative of the other trajectory groups within the same event. For trajectory group A1, 92% of the back trajectories after 24 h have a horizontal error less than or equal to 250 km (Fig. 10a). After 48 h, the distribution of the horizontal errors becomes significantly wider and by 72 h only 31% of the back trajectories have a horizontal error less than 250 km. A significant fraction of the trajectories have a horizontal error greater than 500 km. The

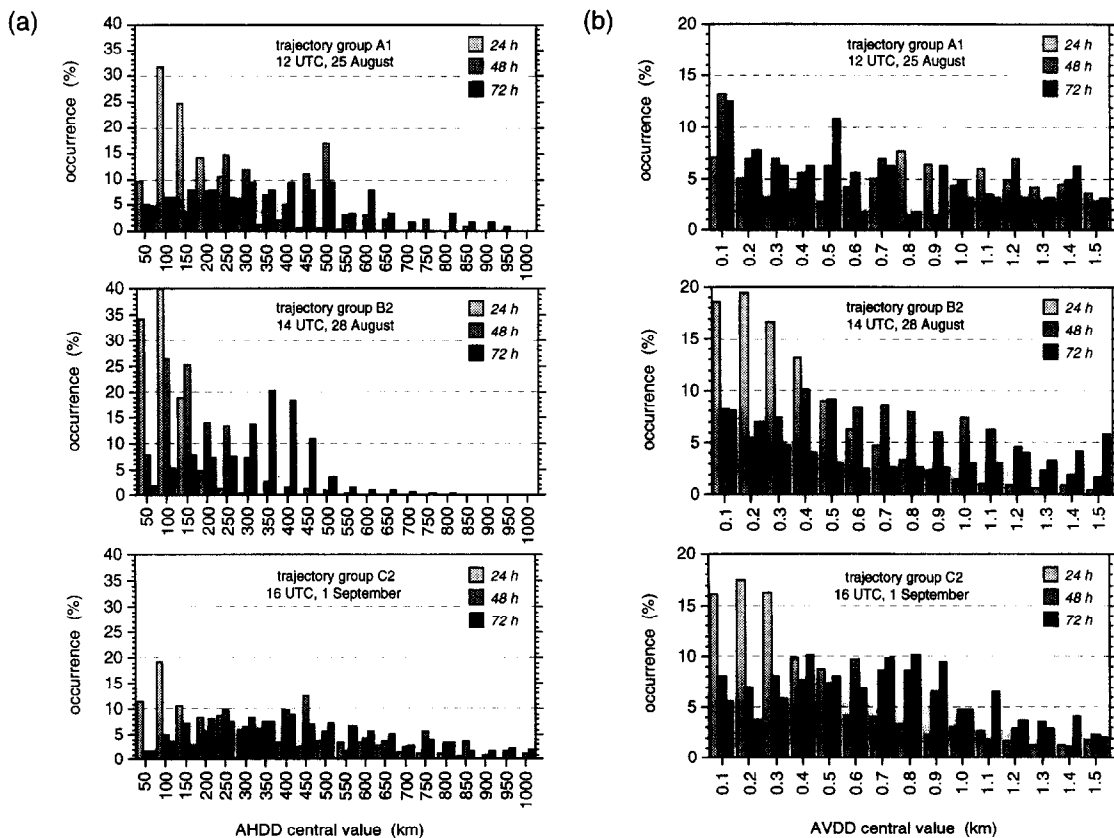


Fig. 10. Histogram of frequency of occurrence vs (a) AHDD and (b) AVDD for back trajectory groups A1, B2, and C2.

distribution for trajectory group B2 is narrower in general and the mean AHDD and AVDD is small, indicating that the back trajectory errors are relatively small for this group compared to the other time periods. At 24 h, 99% of the trajectories have an error of 250 km or less. There are very few trajectories with errors greater than 500 km after 48 h. While there is a peak in the error distribution at 100 km at 24 h for trajectory group C2, the overall distribution at the three time periods is significantly wider than the other groups. The vertical displacement errors in Fig. 10b show that the distribution of the vertical errors increases in time for trajectory groups B2 and C2, but that there is no pattern in the distribution for group A1. At 24 h, 53 and 48% of the back trajectories for groups B2 and C2, respectively, have an error less than or equal to 300 m. As the back trajectories pass over the land areas at longer times, the vertical errors increase and the distribution widens. The results sometimes suggest a reduction in error with time. For example, the fraction of trajectories with an error of 100 m is higher at 48 and 72 h than at 24 h for trajectory group A1 (Fig. 10b). However, the reduction of the average vertical error with time is usually due to fortuitous circumstances. As illustrated by the trajectory in Fig. 7b, the vertical positions of the forward and back trajectories are nearly identical a couple of times (even though they are separated by large horizontal distances) during the transport period due to different atmospheric mechanisms.

6. CONCLUSION

Results from a mesoscale model and a Lagrangian particle dispersion model are used to simulate forward dispersion during high ozone events of the 1993 NARE field campaign. Using particle concentration as a surrogate for ozone mixing ratio, quite good agreement was found between predicted and observed vertical profiles over Yarmouth, Nova Scotia. The peak particle concentrations occurred at nearly the same elevations as the maximum ozone mixing ratios, suggesting that the modeling system is reproducing the atmospheric mechanisms responsible for pollutant layering during this period. Forward trajectories from the dispersion of particles indicated that inhomogeneous convective boundary layer processes over the source regions coupled to synoptic-scale horizontal and vertical transport could explain the layering of pollutants over Yarmouth. The paths described by these forward trajectories were used as the basis for comparison against back trajectories emanating from Yarmouth. Eight time periods corresponding to intensive measurement campaigns by aircraft are selected for detailed analysis.

In all of the events considered, convective boundary layer processes are found to be responsible for mixing a large fraction of the particles upwards before they are advected into the sampling domain by stronger

westerly winds aloft. The corresponding back trajectories had no mechanism to identify these surface source regions, with the consequence that the back trajectories would either pass over the "true" source region, or miss it altogether as a result of locating the particle at an incorrect horizontal position.

A statistical description of thousands of trajectories using the AHDD and AVDD shows that although relatively small errors could occur as far as 750 km upwind of Yarmouth at times, a mean AHDD of 100–400 km and a mean AVDD of 200–1000 m was commonly associated with only 2 days of transport. The mean AHDD and AVDD remained relatively constant between 2 and 3 days, but grew larger again after 3 days of transport and is expected to be even larger for transport times greater than 4 days. The differences between the back and forward trajectories are smaller (but not negligible) in the free atmosphere and within the stable boundary layer over the land and ocean. Large differences between the forward trajectories and their back trajectory counterparts were found to occur because turbulent diffusion processes are irreversible and cannot be included in the back trajectory calculations.

We conclude that the use of back trajectories to identify surface source regions for long-range transport is suitable only for a coarse approximation of the point of origin. Since many chemistry studies employ single or multiple back trajectories to simulate the transport of air pollutants, alternative techniques should be used whenever possible to determine the most likely surface source location. Although several methods have been developed recently to better describe source-receptor relationships (Flesch *et al.*, 1995; Mulholland, 1989; Stohl, 1996; Stohl and Wotawa, 1995; Uliasz, 1993), additional research is necessary to test these methods with tracer data from a variety of field experiments.

Acknowledgements - We appreciate the generosity of Larry Kleinman, Brookhaven National Laboratory, in providing the aircraft data used in this study. This work was supported by the U.S. Department of Energy's Atmospheric Studies in Complex Terrain (ASCOT) Program and Atmospheric Chemistry Program through the Office of Health and Environmental Research (OHER).

REFERENCES

- Anderson B. E., Gregory G. L., Barrick J. D. W., Collins J. E. Jr., Sachse G. W., Bagwell D., Shipham M. C., Bradshaw J. D. and Sandholm S. T. (1993) The impact of U.S. continental outflow on ozone and aerosol distribution over the western Atlantic. *J. geophys. Res.* **98**, 23,477–23,489.
- Angevine W. M., Buhr M. P., Holloway J. S., Trainer M., Parrish D. D., MacPherson J. I., Kok G. L., Schillawski R. D. and Bowlby D. H. (1996) Local meteorological features affecting chemical measurements at a North Atlantic coastal site. *J. geophys. Res.* (to appear).
- Berkowitz C. M., Busness K. M., Chapman E. G., Thorp J. M. and Saylor R. D. (1995) Observations of depleted ozone within the boundary layer of the western North Atlantic. *J. geophys. Res.* **100**, 11,483–11,496.

- Berkowitz C. M., Daum P. H., Spicer C. W. and Busness K. M. (1996) Synoptic patterns associated with the flux of excess ozone to the western North Atlantic. *J. geophys. Res.* (to appear).
- Chock D. P. and Kuo Y.-H. (1990) Comparison of wind-field models using the CAPTEX data. *J. appl. Met.* **29**, 76–91.
- Daum P. H., Kleinman L. I., Newman L., Luke W., Weinstein-Lloyd J., Berkowitz C. M. and Busness K. (1996) Measurements of the chemical and physical properties of plumes of anthropogenic pollutants transported over the North Atlantic during the North Atlantic Regional Experiment. *J. geophys. Res.* (to appear).
- Dickerson R. R., Doddridge B. G., Kelley P. and Rhoads K. P. (1995) Large-scale pollution of the atmosphere over the remote Atlantic Ocean: evidence from Bermuda. *J. geophys. Res.* **100**, 8945–8952.
- Doty K. G. and Perkey D. J. (1993) Sensitivity of trajectory calculations to the temporal frequency of wind data. *Mon. Weath. Rev.* **121**, 387–401.
- Draxler R. R. (1987) Sensitivity of a trajectory model to the spatial and temporal resolution of the meteorological data during CAPTEX. *J. Clim. appl. Met.* **26**, 1577–1588.
- Draxler R. R. (1991) The accuracy of trajectories during ANATEX calculated using dynamic model analyses versus rawinsonde observations. *J. appl. Met.* **30**, 1446–1467.
- Fast J. D. (1995) Mesoscale modeling in areas of highly complex terrain. *J. appl. Met.* **34**, 2762–2782.
- Fast J. D. and Berkowitz C. M. (1996) A modeling study of boundary-layer processes associated with ozone layers observed during the 1993 North Atlantic Regional Experiment. *J. geophys. Res.* (to appear).
- Fast J. D., O'Steen B. L. and Addis R. P. (1995) Advanced atmospheric modeling for emergency response. *J. appl. Met.* **34**, 626–649.
- Flesch, T. K., Wilson, J. D. and Yee E. (1995) Backward-time Lagrangian stochastic dispersion models and their application to estimate gaseous emissions. *J. appl. Met.* **34**, 1320–1332.
- Graber W. K., Andreani-Aksoyoglu S., Keller J. E. and Rosselet C. M. (1995) Multi-parcel Lagrangian model for quantification of influence of Alpine air mass exchange on photo-oxidant production. *Atmospheric Environment* **29**, 2961–2976.
- Haagenson P. L., Gao K. and Kuo Y.-H. (1990) Evaluation of meteorological analyses, simulations and long-range transport calculations using ANATEX surface tracer data. *J. appl. Met.* **29**, 1268–1283.
- Harms D. E., Raman S. and Madala R. V. (1992) An examination of four-dimensional data-assimilation techniques for numerical weather prediction. *Bull. Amer. Met. Soc.* **73**, 425–440.
- Helfand H. M. and Labraga J. C. (1988) Design of a nonsingular level 2.5 second-order closure model for the prediction of atmospheric turbulence. *J. Atmos. Sci.* **45**, 113–132.
- Hurley P. and Physick W. (1991) A Lagrangian particle model of fumigation by breakdown of the nocturnal inversion. *Atmospheric Environment* **25A**, 1313–1325.
- Jacob D. J., Horowitz L. W., Munger J. W., Heikes B. G., Dickerson R. R., Artz R. S. and Keene W. C. (1995) Seasonal transition from NO_x to hydrocarbon-limited conditions for ozone production over the eastern United States in September. *J. geophys. Res.* **100**, 9315–9324.
- Kahl J. D. and Samson P. J. (1986) Uncertainty in trajectory calculations due to low resolution meteorological data. *J. Climate appl. Met.* **25**, 1816–1831.
- Kahl J. D. and Samson P. J. (1988) Trajectory sensitivity to rawinsonde data resolution. *Atmospheric Environment* **22**, 1291–1299.
- Kleinman L. I., Daum P. H., Lee Y.-N., Springston S. R., Newman L., Leaitch W. R., Banic C. M., Isaac G. A. and MacPhearson J. I. (1996a) Measurement of O₃ and related compounds over southern Nova Scotia. Part I: vertical distributions. *J. geophys. Res.* (to appear).
- Kleinman L. I., Daum P. H., Springston S. R., Leaitch W. R., Banic C. M., Isaac G. A., Jobson B. T. and Niki H. (1996b) Measurement of O₃ and related compounds over southern Nova Scotia. Part II: photochemical age and vertical transport. *J. geophys. Res.* (to appear).
- Kuo Y.-H., Skumanich M., Haagenson P. L. and Chang J. S. (1985) The accuracy of trajectory models as revealed by observing simulation experiments. *Mon. Weath. Rev.* **113**, 1852–1867.
- Legg B. J. and Raupach M. R. (1982) Markov-chain simulation of particle dispersion in inhomogeneous flows: The mean drift velocity induced by a gradient in Eulerian velocity variance. *Boundary-Layer Met.* **24**, 3–13.
- McQueen J. T. and Draxler R. R. (1994) Evaluation of model back trajectories of the Kuwait oil fires smoke plume using digital satellite data. *Atmospheric Environment* **28**, 2159–2174.
- Martin D., Mithieux C. and Strauss B. (1987) On the use of the synoptic vertical wind component in a transport trajectory model. *Atmospheric Environment* **21**, 45–52.
- Mellor G. L. and Yamada T. (1982) Development of a turbulent closure model for geophysical fluid problems. *Rev. geophys. Space Phys.* **20**, 851–875.
- Moy L. A., Dickerson R. R. and Ryan W. F. (1994) Relationship between back trajectories and tropospheric trace gas concentrations in rural Virginia. *Atmospheric Environment* **28**, 2789–2799.
- Mukai H., Tanaka A. and Fujii T. (1994) Lead isotope ratios of airborne particulate matter as tracer of long-range transport of air pollutant around Japan. *J. geophys. Res.* **99**, 3737–3726.
- Mulholland M. (1989) An autoregressive atmospheric dispersion model for fitting combined source and receptor data sets. *Atmospheric Environment* **23**, 1443–1458.
- Parrish D. D., Holloway J. S., Trainer M., Murphy P. C., Forbes G. L. and Fehsenfeld F. C. (1993) Export of North American ozone pollution to the North Atlantic Ocean. *Science* **259**, 1436–1439.
- Pielke R. A., Cotton W. R., Walko R. L., Tremback C. J., Lyons W. A., Grasso L. D., Nicholls M. E., Moran M. D., Wesley D. A., Lee T. J. and Copeland J. H. (1992) A comprehensive meteorological modeling system—RAMS. *Met. atmos. Phys.* **49**, 69–91.
- Rolph G. D. and Draxler R. R. (1990) Sensivity of three-dimensional trajectories to the spatial and temporal densities of the wind field. *J. appl. Met.* **29**, 1043–1054.
- Seibert P. (1993) Convergence and accuracy of numerical methods for trajectory calculations. *J. appl. Met.* **32**, 558–566.
- Stauffer D. R. and Seaman N. L. (1994) Multiscale four-dimensional data assimilation. *J. appl. Met.* **33**, 416–434.
- Stohl A. (1996) Trajectory statistics—a new method to establish source-receptor relationships of air pollutants and its application to the transport of particulate sulfate in Europe. *Atmospheric Environment* **30**, 579–587.
- Stohl A. and Kromp-Kolb H. (1994) Origin of ozone in Vienna and surroundings, Austria. *Atmospheric Environment* **28**, 1255–1266.
- Stohl A. and Wotawa G. (1995) A method for computing single trajectories representing boundary layer transport. *Atmospheric Environment* **29**, 3235–3238.
- Stohl A., Wotawa G., Seibert P. and Kromp-Kolb H. (1995) Interpolation errors in wind fields as a function of spatial and temporal resolution and their impact on different types of kinematic trajectories. *J. appl. Met.* **34**, 2149–2165.
- Uliasz, M. (1993) The atmospheric mesoscale dispersion modeling system. *J. appl. Met.* **32**, 139–149.
- Van Dingenen R., Raes F. and Jensen N. R. (1995) Evidence for anthropogenic impact on number concentration and sulfate content of cloud-processed aerosol particles over the North Atlantic. *J. geophys. Res.* **100**, 21,057–21,067.